


Article

Photocatalytic Degradation of Microcystins by TiO₂ Using UV-LED Controlled Periodic Illumination

Olivia M. Schneider ^{1,†}, Robert Liang ^{1,2,*,†} , Leslie Bragg ³, Ivana Jaciw-Zurakowsky ¹, Azar Fattahi ¹, Shasvat Rathod ¹, Peng Peng ⁴, Mark R. Servos ³ and Y. Norman Zhou ^{1,2}

¹ Centre for Advanced Materials Joining, Department of Mechanical and Mechatronics Engineering, University of Waterloo, Waterloo, ON N2L 3G1, Canada; omschnei@edu.uwaterloo.ca (O.M.S.); ivana.jaciwzurakowsky@edu.uwaterloo.ca (I.J.-Z.); azar.fattahi@uwaterloo.ca (A.F.); s2rathod@edu.uwaterloo.ca (S.R.); nzhou@uwaterloo.ca (Y.N.Z.)

² Waterloo Institute of Nanotechnology, University of Waterloo, Waterloo, ON N2L 3G1, Canada

³ Department of Biology, University of Waterloo, Waterloo, ON N2L 3G1, Canada; leslie.bragg@uwaterloo.ca (L.B.); mservos@uwaterloo.ca (M.R.S.)

⁴ School of Mechanical Engineering and Automation, International Research Institute for Multidisciplinary Science, Beihang University, 37 Xueyuan Rd, Beijing 100191, China; peng.peng@uwaterloo.ca

* Correspondence: rliang@uwaterloo.ca; Tel.: +1-519-888-4567 (ext. 33326)

† Denotes equal contribution.

Received: 18 January 2019; Accepted: 11 February 2019; Published: 14 February 2019



Abstract: Toxic microcystins (MCs) produced by freshwater cyanobacteria such as *Microcystis aeruginosa* are of concern because of their negative health and economic impacts globally. An advanced oxidation process using UV/TiO₂ offers a promising treatment option for hazardous organic pollutants such as microcystins. The following work details the successful degradation of MC-LA, MC-LR, and MC-RR using a porous titanium–titanium dioxide (PTT) membrane under UV-LED light. Microcystin quantitation was achieved by sample concentration and subsequent LC–MS/MS analysis. The PTT membrane offers a treatment option that eliminates the need for the additional filtration or separation steps required for traditional catalysts. Controlled periodic illumination was successfully used to decrease the total light exposure time and improve the photonic efficiency for a more cost-effective treatment system. Individual degradation rates were influenced by electrostatic forces between the catalyst and differently charged microcystins, which can potentially be adjusted by modifying the solution pH and the catalyst’s isoelectric point.

Keywords: *Microcystis aeruginosa*; microcystin; controlled periodic illumination; titanium dioxide; advanced oxidation process

1. Introduction

Cyanobacteria are a phylum of phototrophic bacteria capable of producing toxic blooms. *Microcystis aeruginosa* is a common freshwater cyanobacteria which produces microcystins (MC), a group of cyanotoxins with strong hepatotoxic effects. With the increased eutrophication of freshwater resources worldwide, the prevalence of these toxic blooms is a growing concern [1–3]. Over the last several years they have been linked to a variety of both animal and human poisonings globally, including in Canada, Australia, the United Kingdom, China, and Africa [4]. The World Health Organization deems the acceptable level of microcystin-LR, the most common microcystin, in drinking water to be 1 µg L⁻¹ [4]. For example, a review document produced by Health Canada in 2016 concluded that toxic algal blooms impact drinking water safety in the majority of Canadian provinces [5]. These toxic blooms also cause significant economic losses in affected areas by impeding

tourism and fishing, lowering property values, and requiring expensive preventative strategies and monitoring [2,6,7].

Recent studies show that advanced oxidation processes (AOPs) such as ultraviolet (UV) light/TiO₂ photocatalysis can break down microcystins [8–12]. When TiO₂ particles are irradiated by UV light, electrons in the valence band are excited to the conduction band, creating electron–hole pairs. These electron–hole pairs can either undergo redox reactions directly with small organic molecules or with water to form reactive oxygen species (ROS) such as hydroxyl radicals, which then participate in redox reactions with small organic molecules [13–20]. UV/TiO₂ photocatalysis is a promising AOP for treating microcystins in water because the TiO₂ is catalytic, providing a constant oxidant source without having to be replenished, as is the case in UV/H₂O₂ AOPs.

Traditional slurry TiO₂ reactors are impractical for water treatment because they require an additional filtration step to remove the catalyst. In order to address this issue, a porous titanium–titanium dioxide membrane was used in this study. The membrane is made of a porous titanium sheet, oxidized, and calcinated to produce TiO₂ structures on its surface. In order to show the hydroxyl radical production of the catalyst under UV illumination, the conversion of terephthalic acid (TPA) to 2-hydroxyterephthalic acid (HTPA) was quantified by fluorescence [16]. The trade-off of using the membrane is that it has less surface area than the equivalent mass of powder TiO₂, decreasing adsorption and lowering the degradation rate [21,22].

Previous work also suggests that the photonic efficiency of the process can be improved using controlled periodic illumination (CPI) [19,23,24]. The improved efficiency under CPI conditions can be compared to a phenomenon called Parrondo's paradox, where alternating two less favorable conditions results in a more favorable outcome. The improved efficiency, when using a catalyst such as the porous titanium–titanium dioxide (PTT) membranes, can be explained by mass-transfer limitations. Because the membrane has a limited surface area for adsorption, the rate of the reaction may be limited by this surface area at high LED duty cycles [25]. In this case, periodically illuminated lighting conditions (within the mass-transfer limit) will be equally effective. In the case of photon-limited reactions (for example, slurry reactors), mass-transfer limitations would not apply because the reaction rate is faster than the adsorption rate.

Typical light sources such as mercury and xenon lamps require mechanical shutters to produce CPI, take time to warm up, and lack efficiency and reliability. UV-LEDs are ideal light sources in this case because high-frequency CPI can be generated using pulse-width modulation (PWM) through a microcontroller. The microcontroller also allows for easy optimization of the light frequency, including the implementation of dual-frequency profiles that may exhibit a synergistic effect. By decreasing the cumulative light exposure time in UV/TiO₂ photocatalysis, the efficiency of the system and the life span of the light source can be increased without sacrificing performance. A more energy-efficient system would be particularly advantageous for the practical application of larger-scale water treatment.

The following study details the removal of MC-LA, MC-LR, and MC-RR from water using UV/TiO₂ photocatalytic degradation with porous titanium–titanium dioxide membranes. Degradation under each set of conditions, for individual and cumulative microcystin concentrations, was monitored using LC–MS/MS. Controlled periodic illumination at frequencies of 50, 5, 0.5, and dual 0.05 and 25 Hz were all considered, with the goal of improving the photonic efficiency of the AOP.

2. Results and Discussion

2.1. PTT Membrane Characterization

The PTT membrane characterization results have been described in previous works [16,17]. In summary, Raman spectra and XRD indicated mainly anatase TiO₂, with some rutile TiO₂ and titanium. The experimental band-gap energy of 3.0 eV also indicated that the PTT membranes were primarily composed of crystalline TiO₂. The isoelectric point of the PTT membrane was also determined to be 6.0 using a SurPASS™ electrokinetic analyzer.

2.2. TPA Conversion

A summary of the TPA conversion under continuous UV, 0.5, 25, and dual 0.05 and 25 Hz can be seen in Figure 1. As expected, k_1 was highest for continuous UV light because the cumulative UV-LED exposure was twice that of the other lighting conditions. In order to properly compare degradation relative to the electrical energy consumed, electrical energy per order (E_{EO}) was calculated. Although the dual lighting conditions had the lowest degradation rates, they also had the lowest E_{EO} , making dual lighting the most efficient set of conditions for TPA conversion. The other two frequencies tested also had lower E_{EO} values than that for continuous light, making continuous UV-LED exposure the least efficient of the four conditions tested for TPA conversion. These results are in agreement with Parrondo's paradox and show that CPI is a viable method for improving the efficiency of the photocatalytic AOP.

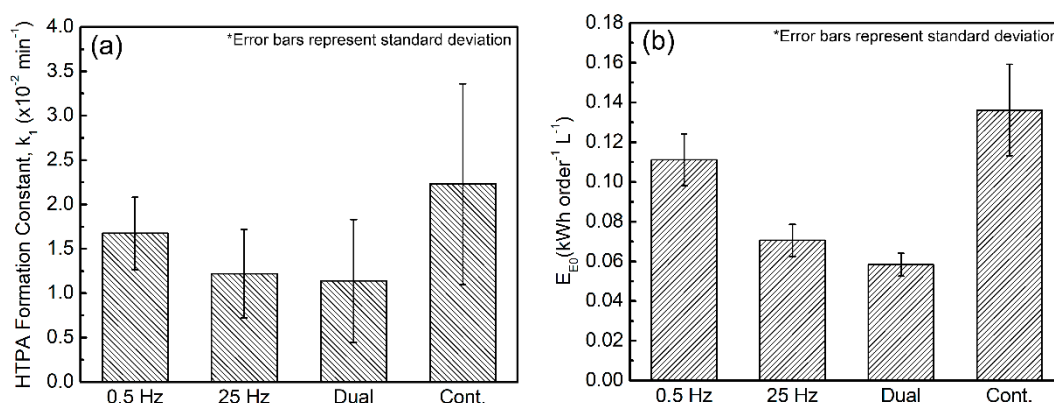


Figure 1. (a) Rate constants and (b) electrical energy per order for terephthalic acid (TPA) conversion under various UV-LED conditions.

2.3. Degradation of Microcystins under Continuous Light

Experiments testing the membrane under dark conditions and testing UV exposure without the membrane showed no degradation of the microcystins (see the Supplementary Information). This verifies that the photocatalytic AOP was responsible for the microcystin degradation. All three microcystins showed successful degradation when treated with UV light and PTT membranes, with a cumulative rate of $-0.00453 \text{ min}^{-1}$. MC-LA degraded the fastest, with a rate of $-0.00841 \text{ min}^{-1}$. Both MC-LR and MC-RR degraded at less than half that rate ($-0.00350 \text{ min}^{-1}$ and $-0.00332 \text{ min}^{-1}$, respectively). This difference in the degradation rate can be explained by the difference in adsorption, which is influenced by relative charge.

The unmodified experimental pH was determined to be 5 and remained consistent throughout the course of the experiment. At this experimental pH, each microcystin has a different charge depending on the variable amino acids in the ring structure. A summary of these charges is included in Table 1. At experimental pH the PTT membrane is positively charged. These relative charges can explain the significant difference seen between degradation rates for MC-LA and MC-LR or MC-RR. In solution, MC-LA is the most oppositely charged to the PTT membrane and experiences the greatest electrostatic attraction. MC-LR is also negatively charged (though not as strongly) and will experience less significant electrostatic attraction. Inversely, MC-RR is positively charged and will experience electrostatic repulsion from the PTT membrane. The increased electrostatic attraction experienced by MC-LA will increase its adsorption onto the PTT membrane and result in a faster degradation rate. Since MC-LR and MC-RR compete with MC-LA for limited adsorption sites on the PTT membrane, the two microcystins that experience less electrostatic attraction will not adsorb as well and will have slower degradation rates. The influence of these interactions is reflected in the relative degradation rates under continuous UV illumination, where MC-LR and MC-RR have degradations rates less than half that of MC-LA.

Table 1. Microcystin charge at experimental pH.

Compound	Charge at pH 5 ^a
MC-LA	−1.9332
MC-LR	−0.9329
MC-RR	0.0567

^a Charge was calculated by chemicalize.org.

These results are consistent with previous studies by Arlos et al. and Liang et al., which showed that electrostatic forces between the pollutant and catalyst have a significant influence on the degradation rate [16,25]. The influence of electrostatic forces demonstrates the importance of considering the pH and the charge of target pollutants when treating water [26]. Degradation rates are highly pH-dependent, so the pH of the water being treated must be considered, especially in practical applications. In future water treatment designs, this information can be used to tune the isoelectric point of the catalyst to improve the degradation of desired pollutants.

2.4. Degradation of Microcystins under CPI

Using UV-LED PWM, the following CPI conditions were examined: 0.5, 5, 50, and dual 0.05 and 25 Hz. The calculated E_{EO} for these conditions, as well as those for continuous UV light for comparison, can be seen in Figure 2. Because MC-LA degraded preferentially to MC-LR and MC-RR, the change in concentration of MC-LR and MC-RR was subtle and lacked linearity (see Table S1 and Figure S1). For this reason, there were significantly larger errors associated with their calculated E_{EO} . As a result, the cumulative microcystin E_{EO} was considered when comparing different lighting conditions. As predicted by the TPA results, several of the controlled periodic illumination conditions presented more energy efficient options. Both the 5 and 0.5 Hz UV lighting had significantly lower E_{EO} than the continuous UV lighting. Dual frequency lighting, which is an equal combination of 0.05 and 25 Hz, had a comparable E_{EO} to continuous UV.

Among the lighting conditions tested, the least degradation overall was observed at 50 Hz (cumulative $k_{app} = -7.83 \times 10^{-4} \text{ min}^{-1}$, see Table S1). Very little degradation of MC-LA and MC-RR occurred, and no degradation of MC-LR occurred (see Figures S1 and S2). Given the low magnitude of degradation and the associated margin of error, it is difficult to discern any trend in degradation between different microcystins under 50 Hz UV illumination, as was done for continuous UV. This significant decrease in overall degradation resulted in a correspondingly high E_{EO} for microcystin degradation under 50 Hz UV. In general, the E_{EO} increased as the frequency increased, meaning lower-frequency lighting conditions were more efficient. In dual lighting, the combination of both high and low frequencies balanced each other and resulted in an insignificant net change relative to continuous UV.

Interestingly, the improvement of reaction efficiency under CPI agrees with Parrondo's paradox. In Parrondo's paradox, alternating between two less favorable conditions yields a more favorable result. In this case, the two less favorable UV-LED conditions were off (which did not contribute to the AOP) and on (which was inefficient). By alternating these two conditions at different frequencies, the time the UV-LED was on decreased by 50%. The favorable outcome was that the E_{EO} under CPI decreased, demonstrating improved efficiency.

Although the PTT membrane provided a more practical option for water treatment, the reduced surface area relative to a slurry reactor imposed mass-transfer limitations. Because the rates of adsorption and desorption to the surface of the catalyst were significantly slower than the rate of electron-hole pair formation and recombination, the process of adsorption and desorption was rate-limiting [24,27]. This had a significant impact on the photonic efficiency of the system. In using CPI, the dark period allowed for the equilibration of the untreated pollutant molecules on adsorption sites, without wasting energy [18,23,28]. This improved the photonic efficiency of the photocatalytic system. The results indicated that CPI is a viable method for improving the efficiency of photocatalytic

AOPs used to treat organic pollutants and toxins, though further optimization of conditions is required. Improving the photonic efficiency of the process makes it more energy efficient and prolongs the life of the light source. These characteristics are particularly attractive in the water treatment industry because they reduce costs.

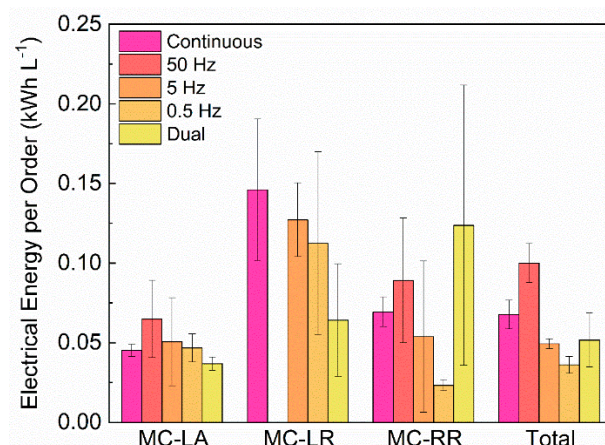


Figure 2. Electrical energy per order for microcystin degradation under continuous and controlled periodic illumination (CPI) conditions.

3. Materials and Methods

3.1. Reagents and Chemicals

Microcystins and nodularin (Cayman Chemicals, Ann Arbor, MI, USA) were dissolved in UHPLC-grade methanol (VWR International, Mississauga, ON, Canada) and stored at $-20\text{ }^{\circ}\text{C}$. PTT membrane synthesis required hydrogen peroxide (Sigma-Aldrich, St. Louis, MO, USA) and 0.254-mm-thick porous titanium (PTi) sheets (Accumet Materials, Ossining, NY, USA). For LC-MS analysis, HPLC-grade ammonium fluoride (Sigma-Aldrich, St. Louis, MO, USA) and HPLC-grade acetonitrile (Thermo Fisher Scientific, Waltham, MA, USA) were used. For measuring hydroxyl radical formation, TPA and sodium hydroxide were purchased from Sigma-Aldrich, St. Louis, MO, USA. Water was purified using a Milli-Q® Integral water purification system (EMD Millipore, Burlington, MA, USA) ($18.2\text{ m}\Omega\cdot\text{cm}$ resistivity at $25\text{ }^{\circ}\text{C}$).

3.2. PTT Membrane Synthesis and Characterization

PTT membrane synthesis and characterization methods are described in previous works [16,17]. In short, PTi membranes were cut into 5-cm diameter discs, cleaned and oxidized in a hydrogen peroxide solution at $80\text{ }^{\circ}\text{C}$, and then calcined at $600\text{ }^{\circ}\text{C}$. Material characterization methods included micro-Raman spectroscopy (He-Ne laser $\lambda = 632.8\text{ nm}$, Renishaw, Wotton-under-Edge, UK), scanning electron microscopy (FE-SEM LEO 1550, Carl Zeiss Microscopy, Jena, Germany), and X-ray diffraction (XPERT-PRO, Malvern Panalytical, Malvern, UK).

3.3. Experimental Setup for Microcystin Degradation

A volume of MC-LA, MC-LR, and MC-RR stock solution was evaporated to dryness under nitrogen gas and then reconstituted to $2\text{ }\mu\text{g/L}$ in MilliQ water for a reaction solution. The PTT membranes were suspended in 0.4-L beakers on metal stands, 1.5 cm under the solution surface with a volume of 0.3 L.

Many studies of UV/TiO₂ photocatalysis use methanol as a carrier solvent when preparing aqueous pollutant solutions [10,16,17,29–35]. More recent studies show that methanol has a significant effect on photocatalytic degradation because it acts as a hydroxyl radical scavenger, even at low

concentrations [36,37]. In order to replicate the effects of methanol under typical experimental conditions, all reactions were conducted in 0.02% methanol.

Reactions took place using a UV-LED source with an average irradiance of 2.18 mW cm^{-2} under continuous illumination and 1.08 mW cm^{-2} under a 50% duty cycle (measured 18 cm from the light source using Thorlabs PM100-USB power meter, S120VC 200–1100 nm, 50 mW). Reaction solutions were stirred at 600 rpm. The solution surface was initially 10.5 cm below the light source. A diagram of the reaction setup is shown in Figure 3a with the UV-LED (LED-Engin LZ1, 1000 mA) spectral power distribution peaking at 365 nm and the total radiation included angle of 105° (90% of the total radiant flux).

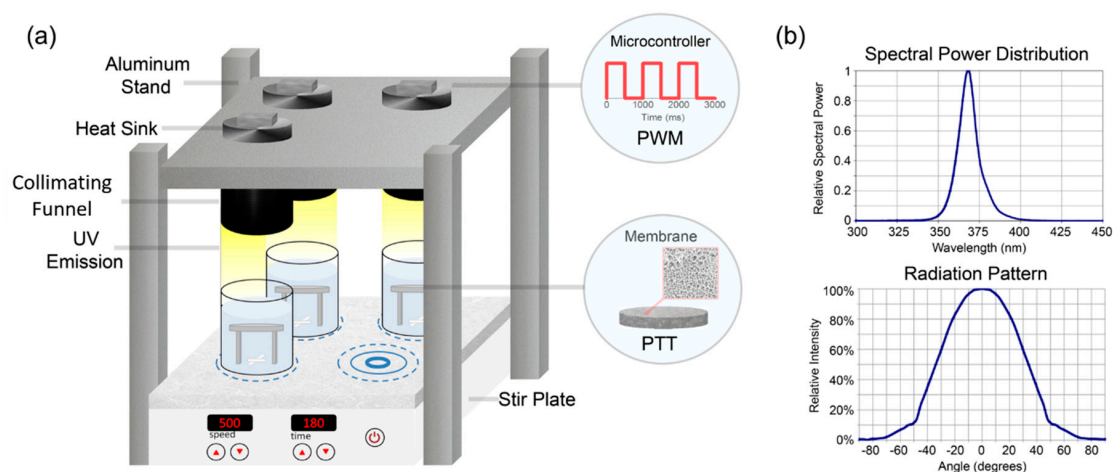


Figure 3. (a) Experimental setup for UV/TiO₂ reactors and (b) UV-LED spectral power distribution and radiation pattern. Abbreviations: PWM—pulse-width modulation, PTT—porous titanium–titanium dioxide.

Reactions were equilibrated in the dark for 1 h before UV-LED irradiation, with a total reaction time of 6 h. Samples of 4 mL were taken every hour. Each set of conditions was repeated in triplicate. Arduino microcontrollers and LEDSEEDUINO LED current drivers were used to program the UV-LEDs for 0.5, 5, and 50 Hz as well as a dual frequency (0.05 and 25 Hz alternating for equal periods). The pulsed-width modulation script used to program the different conditions can be found in the Supplementary Information. All UV-LED flashing sequences had a duty cycle of 50%. The duty cycle is the ratio of the time on to the time off, as described by the following equation:

$$D = \frac{PW}{T} \times 100\%$$

where D is the duty cycle expressed as a percentage, PW is the pulse width duration, and T is the period of the wave.

At low adsorbate concentrations, the following equation can be used to approximate Langmuir–Hinshelwood kinetics [38]:

$$-r = \frac{dC}{dt} = -k_{app}C.$$

The equation can then be rearranged and integrated to give the following [25]:

$$\ln\left(\frac{C}{C_0}\right) = k_{app}t$$

where C (g L^{-1}) is the analyte concentration at time t (min), C_0 (g L^{-1}) is the initial analyte concentration at $t = 0$, and k_{app} (min^{-1}) is the apparent kinetic rate. The slope of a plot of the equation gives the

k_{app} . OriginLabPro (version 8.0, OriginLab, Northhampton, MA, USA, 2018) was used to complete the linear regression analysis to determine the rates for cumulative and individual compounds.

3.4. Experimental Setup for TPA Conversion

The experimental method is derived from previous work [16]. In brief, a solution of 5 mM TPA was made in 6 mM NaOH. Under the same conditions as described in the previous section, 300 mL of this solution was placed in a beaker with a PTT membrane. UV-LED irradiation began after a 1-h dark equilibration, and samples were taken at various time points over 4 h. The following lighting conditions were tested: Continuous, 0.05, 25, and dual 0.05 and 25 Hz. All frequencies were programmed with a duty cycle of 50%. HTPA concentrations were quantified by fluorescence using a plate reader (SpectraMax M3, Molecular Devices, San Jose, CA, USA) with an excitation wavelength of 315 nm and emission from 350 nm to 550 nm. The intensity value was taken from the peak of the spectrum.

HTPA was the first degradation product of TPA, so its concentration increased sharply at the beginning of the reaction. As more HTPA was produced, it also degraded into more oxidized products. These rates can be described by the following kinetic model [39]:

$$C_{HTPA} = \frac{k_1}{k_2} (1 - e^{-k_2 t})$$

where k_1 is the zeroth-order rate of HTPA formation, k_2 is the pseudo first-order degradation rate of HTPA, C_{HTPA} is the concentration of HTPA in mol L⁻¹, and t is time in minutes.

3.5. Electrical Energy per Order

To more accurately compare the efficiency of lighting conditions with different duty cycles, electrical energy per order (E_{EO}) was calculated. E_{EO} is the energy in kWh needed to decrease the microcystin or TPA concentration by one order of magnitude in a liter of water. E_{EO} was calculated by the following equations [40,41]:

$$E_{EO}(MC) = \frac{1000 \cdot P \cdot t}{V \cdot \log\left(\frac{C_i}{C_f}\right)}$$

$$E_{EO}(HTPA) = \frac{1000 \cdot P \cdot t}{V \cdot k_2}$$

where P is the power dissipated over the treatment process in kW, t is the reaction time in min, V is the reaction volume in L, k_2 is the degradation rate of HTPA, and C_i and C_f are the initial and final microcystin concentrations, respectively.

3.6. Sample Preparation and Analysis

Each 4-mL sample was spiked with nodularin (NOD), a toxin similar in structure to microcystins, to 0.8 µg L⁻¹ for an internal standard [1]. The spiked samples were then evaporated to dryness in a Rocket Evaporator (Thermo Scientific) and reconstituted in 160 µL of UHPLC-grade methanol. Prepared samples were stored at -20 °C until analysis.

Microcystin quantitation was achieved with LC-MS/MS using an Agilent 1200 HPLC and 3200 quadrupole ion trap (QTRAP) mass spectrometer with electrospray ionization (ABSciex). Specific mass spectrometry parameters are summarized in Table 2. In order to achieve separation, a Poroshell 120 SB-C18 column (4.6 × 150 mm, 2.7 µm, Agilent Technologies) was used with 0.5 mM ammonium fluoride and acetonitrile (ACN) at 1 mL min⁻¹ and 40 °C, with 20-µL sample injections. For the mobile phase gradient, 10% ACN was held for 0.5 min, which was increased to 100% ACN over 4.5 min and held for 1 min. The mobile phase composition was then returned to 10% ACN over 0.5 min and equilibrated for 3.5 min before the next injection. The calibration curves for each microcystin were linear from 0.5 to 500 µg L⁻¹.

Table 2. Mass spectrometry parameters for the detection of microcystins.

	Q1 ^a (Da)	Q3 ^b (Da)	Time (ms)	DP ^c (volts)	EP ^d (volts)	CE ^e (volts)	CXP ^f (volts)	CEP ^g (volts)	Retention Time (min)
NOD	825.563	135.3	150	96	12	75	4	40	4.55
MC-LA	911.395	135.2	150	51	12	81	4	36	4.62
MC-LR	995.699	135.1	150	116	12	99	4	36	4.67
MC-RR	519.960	135.2	150	131	7	41	4	26	4.88

^a First quadrupole, ^b third quadrupole, ^c declustering potential, ^d entrance potential, ^e collision energy, ^f collision cell exit potential, and ^g collision cell entrance potential.

4. Conclusions

In this study three common microcystins, MC-LA, MC-LR, and MC-RR, were successfully degraded in water using a UV/TiO₂ photocatalytic AOP. E_{EO} values calculated for TPA conversion determined continuous UV-LED illumination to be less efficient than all the CPI conditions tested, demonstrating the potential of CPI to improve the efficiency of the photocatalytic AOP. Under continuous illumination, the negatively charged MC-LA degraded at more than twice the rate of MC-LR or MC-RR because it preferentially adsorbed onto the positive PTT membrane catalyst. The pH dependence of the degradation rates suggests that the isoelectric point of the catalyst can be tuned to improve the degradation of target pollutants in water of a known pH, given the compound charges. CPI conditions of 0.5, 5, and 50 Hz as well as dual 0.5 and 25 Hz with a 50% duty cycle were also examined for treating microcystins. When considering the cumulative microcystin solution, the 0.5 and 5 Hz CPI conditions were determined to be more efficient than continuous UV light based on the calculated E_{EO}. These results can be explained by mass-transfer limitations, where the rate of adsorption and desorption onto the surface of the catalyst limits photonic efficiency. The results of this work indicate that the use of CPI has the potential to improve the energy efficiency and light source life span in photocatalytic AOPs and is worth further investigation. Improving these parameters makes photocatalytic AOPs more attractive as a large-scale water treatment solution because they have the potential to greatly decrease costs.

Supplementary Materials: The following are available online at <http://www.mdpi.com/2073-4344/9/2/181/s1>, Table S1: Calculated degradation rates. Poor fit with the linear regression model due to insignificant degradation is seen in membrane-only and UV-only conditions, as well as in 50 Hz MC-LR; Figure S1: Change in microcystin concentration over the course of various UV/TiO₂ treatments; Figure S2: Linear regression plots for the calculation of degradation rate; Figure S3: Chromatogram demonstrating the separation of MC-LA, MC-LR, MC-RR, and NOD.

Author Contributions: Conceptualization, R.L.; methodology, O.M.S. and L.B.; investigation, O.M.S., A.F., and I.J.-Z.; data curation, O.M.S. and S.R.; writing—original draft preparation, O.M.S.; writing—review and editing, O.M.S., A.F., S.R., and R.L.; visualization, R.L.; supervision, Y.N.Z., P.P. and M.R.S.; funding acquisition, Y.N.Z., M.R.S., and R.L.

Funding: This research was funded by the Natural Sciences and Engineering Research Council of Canada (grant number: STPG-494554-2016) through a strategic project grant and the Schwartz–Reisman Foundation through the Waterloo Institute of Nanotechnology—Technion University grant.

Acknowledgments: The authors would like to thank the Natural Sciences and Engineering Research Council of Canada, the Schwartz–Reisman Foundation, and Waterloo Institute of Nanotechnology for their financial support.

Conflicts of Interest: The authors have no conflict of interest to declare.

References

1. Dawson, R.M. The Toxicology of Microcystins. *Toxicon* **1998**, *36*, 953–962. [CrossRef]
2. Merel, S.; Walker, D.; Chicana, R.; Snyder, S.; Baurès, E.; Thomas, O. State of knowledge and concerns on cyanobacterial blooms and cyanotoxins. *Environ. Int.* **2013**, *59*, 303–327. [CrossRef] [PubMed]
3. Umehara, A.; Takahashi, T.; Komorita, T.; Orita, R.; Chio, J.-W.; Takenaka, R.; Mabuchi, R.; Park, H.-D.; Tsutsumi, H. Widespread dispersal and bio-accumulation of toxic microcystins in benthic marine ecosystems. *Chemosphere* **2017**, *167*, 492–500. [CrossRef] [PubMed]

4. Chambon, P.; Lund, U.; Galal-Gorchev, H.; Ohanian, E. *Guidelines for Drinking-Water Quality Volume 2—Health Criteria and Other Supporting Information*, 2nd ed.; Kenny, J., Galal-Gorchev, H., Eds.; World Health Organisation: Geneva, Switzerland, 1998; Volume 2.
5. Committee on Drinking Water. *Cyanobacterial Toxins in Drinking Water*; Committee on Drinking Water: Ottawa, ON, Canada, 2016.
6. Wolf, D.; Klaiber, H.A. Bloom and bust: Toxic algae's impact on nearby property values. *Ecol. Econ.* **2017**, *135*, 209–221. [[CrossRef](#)]
7. Dyson, K.; Huppert, D.D. Regional economic impacts of razor clam beach closures due to harmful algal blooms (HABs) on the Pacific coast of Washington. *Harmful Algae* **2010**, *9*, 264–271. [[CrossRef](#)]
8. Sharma, V.K.; Triantis, T.M.; Antoniou, M.G.; He, X.; Pelaez, M.; Han, C.; Song, W.; O'shea, K.E.; De La Cruz, A.A.; Kaloudis, T.; et al. Destruction of microcystins by conventional and advanced oxidation processes: A review. *Sep. Purif. Technol.* **2012**, *91*, 3–17. [[CrossRef](#)]
9. Liu, I.; Lawton, L.A.; Bahnemann, D.W.; Liu, L.; Proft, B.; Robertson, P.K.J. The photocatalytic decomposition of microcystin-LR using selected titanium dioxide materials. *Chemosphere* **2009**, *76*, 549–553. [[CrossRef](#)] [[PubMed](#)]
10. Shephard, G.S.; Om, S.S.O.; De Villiers, D.; Engelbrecht, W.J.; E El, G.; Wessels, F.S. Degradation of microcystin toxins in a falling film photocatalytic reactor with immobilized titanium dioxide catalyst. *Water Res.* **2002**, *36*, 140–146. [[CrossRef](#)]
11. Cornish, B.J.P.A.; Lawton, L.A.; Robertson, P.K.J. Hydrogen peroxide enhanced photocatalytic oxidation of microcystin-LR using titanium dioxide. *Appl. Catal. B Environ.* **2000**, *25*, 59–67. [[CrossRef](#)]
12. Lawton, L.A.; Robertson, P.K.J.; Cornish, B.J.P.A.; Marr, I.L.; Jaspars, M. Processes influencing surface interaction and photocatalytic destruction of microcystins on titanium dioxide photocatalysts. *J. Catal.* **2003**, *213*, 109–113. [[CrossRef](#)]
13. Rizzo, L.; Meric, S.; Guida, M.; Kassinos, D.; Belgiorno, V. Heterogenous photocatalytic degradation kinetics and detoxification of an urban wastewater treatment plant effluent contaminated with pharmaceuticals. *Water Res.* **2009**, *43*, 4070–4078. [[CrossRef](#)] [[PubMed](#)]
14. Liang, R.; Hu, A.; Li, W.; Zhou, Y.N. Enhanced degradation of persistent pharmaceuticals found in wastewater treatment effluents using TiO₂ nanobelt photocatalysts. *J. Nanopart. Res.* **2013**, *15*, 1990. [[CrossRef](#)]
15. Martínez, C.; Canle L., M.; Fernández, M.I.; Santaballa, J.A.; Faria, J. Aqueous degradation of diclofenac by heterogeneous photocatalysis using nanostructured materials. *Appl. Catal. B Environ.* **2011**, *107*, 110–118. [[CrossRef](#)]
16. Arlos, M.J.; Liang, R.; Hatat-Fraile, M.M.; Bragg, L.M.; Zhou, N.Y.; Servos, M.R.; Andrews, S.A. Photocatalytic decomposition of selected estrogens and their estrogenic activity by UV-LED irradiated TiO₂ immobilized on porous titanium sheets via thermal-chemical oxidation. *J. Hazard. Mater.* **2016**, *318*, 541–550. [[CrossRef](#)] [[PubMed](#)]
17. Arlos, M.J.; Hatat-Fraile, M.M.; Liang, R.; Bragg, L.M.; Zhou, N.Y.; Andrews, S.A.; Servos, M.R. Photocatalytic decomposition of organic micropollutants using immobilized TiO₂ having different isoelectric points. *Water Res.* **2016**, *101*, 351–361. [[CrossRef](#)] [[PubMed](#)]
18. Ku, Y.; Shiu, S.-J.; Wu, H.-C. Decomposition of dimethyl phthalate in aqueous solution by UV-LED/TiO₂ process under periodic illumination. *J. Photochem. Photobiol. A Chem.* **2017**, *332*, 299–305. [[CrossRef](#)]
19. Buechler, K.J.; Nam, C.H.; Zawistowski, T.M.; Noble, R.D.; Koval, C.A. Design and Evaluation of a Novel-Controlled Periodic Illumination Reactor To Study Photocatalysis. *Ind. Eng. Chem. Res.* **1999**, *38*, 1258–1263. [[CrossRef](#)]
20. Schneider, J.; Matsuoka, M.; Takeuchi, M.; Zhang, J.; Horiuchi, Y.; Anpo, M.; Bahnemann, D.W. Understanding TiO₂ Photocatalysis: Mechanisms and Materials. *Chem. Rev.* **2014**, *114*, 9919–9986. [[CrossRef](#)]
21. Manassero, A.; Satuf, M.L.; Alfano, O.M. Photocatalytic reactors with suspended and immobilized TiO₂: Comparative efficiency evaluation. *Chem. Eng. J.* **2017**, *326*, 29–36. [[CrossRef](#)]
22. Hegedűs, P.; Szabó-Bárdos, E.; Horváth, O.; Szabó, P.; Horváth, K. Investigation of a TiO₂ photocatalyst immobilized with poly(vinyl alcohol). *Catal. Today* **2017**, *284*, 179–186. [[CrossRef](#)]
23. Szechowski, J.G.; Koval, C.A.; Noble, R.D. Evidence of critical illumination and dark recovery times for increasing the photoefficiency of aqueous heterogeneous photocatalysis. *J. Photochem. Photobiol. A Chem.* **1993**, *74*, 273–278. [[CrossRef](#)]
24. Tokode, O.; Prabhu, R.; Lawton, L.A.; Robertson, P.K.J. Controlled periodic illumination in semiconductor photocatalysis. *J. Photochem. Photobiol. A Chem.* **2016**, *319–320*, 96–106. [[CrossRef](#)]

25. Liang, R.; Van Leuwen, J.C.; Bragg, L.M.; Arlos, M.J.; Li Chun Fong, L.C.M.; Schneider, O.M.; Peng, P.; Servos, M.R.; Zhou, Y.N. Utilizing UV-LED pulse width modulation on TiO₂ advanced oxidation processes to enhance the decomposition efficiency of pharmaceutical micropollutants. *Chem. Eng. J.* **2019**, *361*, 439–449. [[CrossRef](#)]
26. Friedmann, D.; Mendive, C.; Bahnemann, D. Environmental TiO₂ for water treatment: Parameters affecting the kinetics and mechanisms of photocatalysis. *Appl. Catal. B Environ.* **2010**, *99*, 398–406. [[CrossRef](#)]
27. Memming, R. Photoinduced charge transfer processes at semiconductor electrodes and particles. In *Topics in Current Chemistry*; Springer: Berlin/Heidelberg, Germany, 1994; Volume 169, pp. 105–181, ISBN 978-3-540-57565-8.
28. Sczechowski, J.G.; Koval, C.A.; Noble, R.D. A Taylor vortex reactor for heterogeneous photocatalysis. *Chem. Eng. Sci.* **1995**, *50*, 3163–3173. [[CrossRef](#)]
29. Miranda-García, N.; Maldonado, M.I.; Coronado, J.M.; Malato, S. Degradation study of 15 emerging contaminants at low concentration by immobilized TiO₂ in a pilot plant. *Catal. Today* **2010**, *151*, 107–113. [[CrossRef](#)]
30. Miranda-García, N.; Suárez, S.; Sánchez, B.; Coronado, J.M.; Malato, S.; Maldonado, M.I. Photocatalytic degradation of emerging contaminants in municipal wastewater treatment plant effluents using immobilized TiO₂ in a solar pilot plant. *Appl. Catal. B Environ.* **2011**, *103*, 294–301. [[CrossRef](#)]
31. Sun, W.; Li, S.; Mai, J.; Ni, J. Initial photocatalytic degradation intermediates/pathways of 17 α -ethynylestradiol: Effect of pH and methanol. *Chemosphere* **2010**, *81*, 92–99. [[CrossRef](#)] [[PubMed](#)]
32. Nasuhoglu, D.; Berk, D.; Yargeau, V. Photocatalytic removal of 17 α -ethynylestradiol (EE2) and levonorgestrel (LNG) from contraceptive pill manufacturing plant wastewater under UVC radiation. *Chem. Eng. J.* **2012**, *185–186*, 52–60. [[CrossRef](#)]
33. Kralchevska, R.; Milanova, M.; Bistan, M.; Pintar, A.; Todorovsky, D. The photocatalytic degradation of 17 α -ethynylestradiol by pure and carbon nanotubes modified TiO₂ under UVC illumination. *Open Chem.* **2012**, *10*, 1137–1148. [[CrossRef](#)]
34. Marinho, B.A.; de Liz, M.V.; Lopes Tiburtius, E.R.; Nagata, N.; Peralta-Zamora, P.; Iguchi, T.; Kubota, Y.; Fujishima, A. TiO₂ and ZnO mediated photocatalytic degradation of E2 and EE2 estrogens. *Photochem. Photobiol. Sci.* **2013**, *12*, 678–683. [[CrossRef](#)] [[PubMed](#)]
35. Fernández, R.L.; McDonald, J.A.; Khan, S.J.; Le-Clech, P. Removal of pharmaceuticals and endocrine disrupting chemicals by a submerged membrane photocatalysis reactor (MPR). *Sep. Purif. Technol.* **2014**, *127*, 131–139. [[CrossRef](#)]
36. Nosaka, Y.; Nosaka, A.Y. *Photocatalysis and Water Purification: From Fundamentals to Recent Applications*; John Wiley & Sons: Hoboken, NJ, USA, 2013; pp. 3–23.
37. Paul, T.; Miller, P.L.; Strathmann, T.J. Visible-light-mediated TiO₂ photocatalysis of fluoroquinolone antibacterial agents. *Environ. Sci. Technol.* **2007**, *41*, 4720–4727. [[CrossRef](#)] [[PubMed](#)]
38. Turchi, C.S.; Ollis, D.F. Photocatalytic degradation of organic water contaminants: Mechanisms involving hydroxyl radical attack. *J. Catal.* **1990**, *122*, 178–192. [[CrossRef](#)]
39. Cernigoj, U.; Kete, M.; Stangar, U.L. Development of a fluorescence-based method for evaluation of self-cleaning properties of photocatalytic layers. *Catal. Today* **2010**, *151*, 46. [[CrossRef](#)]
40. Gora, S.; Liang, R.; Zhou, Y.N.; Andrews, S. Settleable engineered titanium dioxide nanomaterials for the removal of natural organic matter from drinking water. *Chem. Eng. J.* **2018**, *334*, 638–649. [[CrossRef](#)]
41. Liang, R.; Li Chun Fong, L.C.M.; Arlos, M.J.; Van Leeuwen, J.; Shahnam, E.; Peng, P.; Servos, M.R.; Zhou, Y.N. Photocatalytic degradation using one-dimensional TiO₂ and Ag-TiO₂ nanobelts under UV-LED controlled periodic illumination. *J. Environ. Chem. Eng.* **2017**, *5*, 4365–4373. [[CrossRef](#)]

